

Dissociation and ionization of an HD⁺ beam induced by intense 395-nm ultrashort laser pulses

J. McKenna, A. M. Saylor, B. Gaire, Nora G. Johnson, E. Parke, K. D. Carnes, B. D. Esry, and I. Ben-Itzhak
J.R. Macdonald Laboratory, Department of Physics, Kansas State University, Manhattan, Kansas 66506, USA
 (Received 28 June 2009; published 26 August 2009)

The majority of research on intense ($\sim 10^{14}$ W/cm²) ultrashort (<100 fs) laser-molecule interactions has been focused on studies of H₂⁺ fragmentation, mainly due to its elemental structure. So far the bulk of this work has been conducted using near infrared light while studies at shorter wavelengths are comparatively scarce. We report a detailed investigation of the interaction of 395 nm, 40 fs pulses with an HD⁺ molecular-ion beam, measured using a coincidence three-dimensional momentum imaging technique. This allows us to clearly discriminate dissociation and ionization channels. From the kinetic energy and angular distributions, insight is gained into the intensity dependence of the main breakup processes. We observe the onset of above-threshold dissociation above 10^{14} W/cm², a higher intensity than required for 790 nm due to a smaller transition dipole moment for the low vibrational states probed at 395 nm. Ionization spectra display structure consistent with the above-threshold Coulomb explosion mechanism that we have proposed [B. D. Esry *et al.*, Phys. Rev. Lett. **97**, 013003 (2006)].

DOI: [10.1103/PhysRevA.80.023421](https://doi.org/10.1103/PhysRevA.80.023421)

PACS number(s): 33.80.Wz, 42.50.Hz

I. INTRODUCTION

The past two decades have seen considerable advances in the generation of intense, ultrashort, visible, and infrared laser pulses. These have been used to probe atoms, molecules, and clusters in the regime where the electric field of the laser generates a nonlinear response from the system being probed. In particular, the dynamics of molecules have proven to be rich [1]. A broad and deep understanding of molecular behavior is fundamental in advancing many vibrant areas of science including high-harmonic generation [2], molecular alignment [3], state-selective control of a molecular reaction [4], and molecular imaging [5,6].

To date, many of the important molecular processes have been revealed through studies on the simplest molecular system, H₂⁺. These studies have included a mixture of theory and experiment, the latter being the focus of this paper. The earliest experiments were conducted using H₂ as a precursor molecule and forming H₂⁺ through laser-induced ionization. Typically, H₂⁺ was probed using the same pulse (e.g., [7–9]) although some recent studies have used a time-delayed second (probe) pulse [10–19]. These studies on H₂ have led to the discovery of some of the important molecular processes known to occur in intense fields. In bond-softening (BS) [7,20,21], the molecular bond is “weakened” by the laser field leading to dissociation. In vibrational trapping (VT) [18,22–27], also known as bond hardening (BH), the molecular wave packet is trapped in a laser-induced potential well and can lead to a counterintuitive stabilization of the molecular bond with increasing laser intensity. Below-threshold dissociation (BTD) [28,29] may also result from VT where the molecular wave packet gets released onto a dissociative potential with fewer photons absorbed than generally considered the minimum to dissociate. Above-threshold dissociation (ATD) [20,21,30] is used to describe the dissociation of a molecule through the absorption of an excess number of photons—in analogy to above-threshold ionization [31]. When ionization is enhanced at an elongated critical internuclear distance the process is referred to as

charge-resonance enhanced ionization (CREI) [32–36]. The experimental observation of these effects have been either instigated or confirmed through extensive theoretical work over the years [27,37–48].

In addition to the work on H₂, recent years have seen the development of H₂⁺ molecular ion-beam studies [30,49–60]. This work was pioneered by Figger *et al.* [49] and Williams *et al.* [50], while shortly thereafter our group advanced this initial work by extending the study to kinematically complete measurements of the heavy molecular fragments using a coincidence three-dimensional (3D) momentum imaging technique [53,54]. The ion-beam studies have in many ways complemented the work on the neutral H₂ target. Further progress in this area using an ion-beam target has seen clear vibrational resolution in dissociation spectra [49,51–55,59,60], vibrationally cold studies on an HD⁺ target [58], and has provided direct evidence for above-threshold Coulomb explosion (ATCE) [56].

Naturally, the majority of experimental work on H₂⁺, particularly in the last decade, has been conducted using ~ 800 nm wavelengths due to the accessibility of Ti:sapphire systems, now available as commercial tabletop lasers. As a result, experimental studies using intense light sources at short wavelengths (below 500 nm) and short pulse duration (<500 fs) have been relatively scarce. Of particular note, Thompson *et al.* [61] conducted a detailed exploration of H₂ at 375 nm (85 fs), compared to 750 nm (55 fs), and observed predominantly BS dissociation at 375 nm at intensities up to 7.6×10^{14} W/cm², as well as weak undulations in the Coulomb explosion (CE) channel that they attributed to enhanced ionization (CREI). Posthumus *et al.* [28], who investigated VT in H₂⁺ produced from H₂ in the same laser pulses, observed signs of BTD via a zero-photon dissociation (ZPD) path using 266 nm (250 fs) pulses, with weaker signatures using 400 nm pulses, although recently an alternative explanation of their 266 nm data has been provided by Posthumus *et al.* [62]. Talebpour *et al.* [63] found exciting evidence for perpendicular dissociative ionization of D₂ via high-lying excited states of D₂⁺ at 400 nm (300 fs) that was

not present at 800 nm. In addition, there have been a few two-color experiments where the fundamental and second-harmonic wavelengths of the laser system were mixed [61,64].

Work at short wavelengths using an ion-beam target is even sparser. So far there have been only two reported measurements, one for dissociation and one for ionization, each limited to a single intensity. Sändig *et al.* [49] reported on dissociation of H_2^+ using 392 nm (120 and 200 fs) pulses at 6×10^{13} W/cm² and observed a single broad peak in the kinetic-energy release (KER) distribution, without clear vibrational structure (unlike at 785 nm), which can be identified as BS. In addition, Esry *et al.* [56] studied the ionization channel of H_2^+ using 395 nm (75 fs) pulses and reported evidence for ATCE near the appearance intensity (1.8×10^{14} W/cm²) for ionization.

The goal of the present work is to build upon these earlier investigations of the hydrogen molecular ion at short wavelengths. Using a coincidence 3D momentum imaging technique [53,54], we examine in detail the dissociation and ionization of HD^+ using intense 395 nm and 40 fs pulses over the intensity range 3×10^{13} – 2×10^{14} W/cm². The dissociation spectra are compared with those using 790 nm light under similar conditions. We reveal clear evidence of ATD at this wavelength, elucidated using an intensity difference spectra (IDS) technique [65,66]. We also present evidence for ATCE of HD^+ , in conjunction with that observed previously for H_2^+ [56]. Where appropriate, we employ the Floquet picture to discuss the relevant physics.

Our choice of target, HD^+ , offers an interesting alternative to the more widely explored H_2^+ and D_2^+ . As HD^+ is heteronuclear, the molecular symmetry is broken allowing direct absorption of even, as well as odd, numbers of photons in the transition between all states. This opens the prospect of studying the elusive direct two-photon dissociation pathway that is absent in the other homonuclear hydrogenic molecules. In addition, our coincidence technique allows us to distinguish the $\text{H}^+ + \text{D}$ and $\text{H} + \text{D}^+$ dissociation channels allowing a complete measurement, although one does not expect there to be a significant difference between these two channels.

II. EXPERIMENTAL ARRANGEMENT

Details on our experimental arrangement may be found in our previous communications [53,54]. Nonetheless, for completeness we will recap the essential details relevant to the present study. The HD^+ ions are produced in an electron-cyclotron resonance (ECR) ion source through electron impact on HD molecules. Such a mechanism forms the HD^+ ions in a vibrational distribution of states in close accord with the Franck-Condon principle [67,68]. The ions are accelerated to 9 keV energy and momentum selected through consecutive 25° and 60° bending magnets for transportation to the interaction region with the laser. Electrostatic deflection and focusing elements are used to guide and collimate the beam through a pair of four-jaw slits. We estimate the ion-beam cross-section size at the point of interaction to be approximately 0.6×0.6 mm.

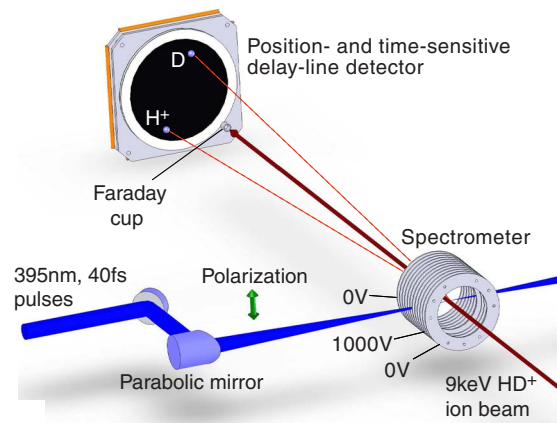


FIG. 1. (Color online) Schematic of the laser-ion-beam interaction region and detection setup. The beams cross within a region of applied electric field that accelerates the charged fragments toward the detector so that the H^+ , D^+ , and neutral fragments can all be distinguished by their flight time to the detector.

In the interaction region, the ion-beam and the focused laser-beam cross at 90° to one another (see schematic outline in Fig. 1). The polarization axis of the laser is approximately orthogonal to the ion-beam propagation direction. As breakup of HD^+ is predominantly along the polarization axis (as we will show), the center-of-mass momentum imparted to the fragments from laser-induced dissociation and ionization is mostly in the transverse direction to ion-beam propagation. This gives the fragments a large spatial spread in the plane perpendicular to the ion-beam allowing them to escape the collection solid angle of the Faraday cup (see Fig. 1).

To detect the fragments we use a position- and time-sensitive detector that we operate in event mode. The detector consists of a pair of 80-mm-diameter microchannel plates with a delay-line anode. Using the position and time-of-flight information we can retrieve the 3D momentum vectors of each fragment that hits the detector. The primary HD^+ beam is collected in a small Faraday cup (2 mm diameter) positioned along the axis of the apparatus. Only fragments with low energy in the transverse direction (≤ 0.02 eV) are lost due to blocking by the Faraday cup. As the typical fragment energy is ≥ 0.02 eV, and they dissociate predominantly along the polarization axis in the transverse direction, the number of lost fragments is few.

To distinguish between fragments with different mass-to-charge ratios (i.e., among H^+ , D^+ , and the neutrals, H and D), we use a spectrometer approximately aligned to the ion-beam direction that creates a weak axial electric field in the interaction region. A potential difference of ~ 800 V applied between the interaction point and the exit of the spectrometer accelerates the charged fragments and thus separates the H^+ , D^+ , and neutral particles in flight time. Therefore, by limiting the number of fragmentation events per laser shot to much less than 1 on average (which naturally occurs due to the thin target density of the ion beam), one can detect the fragments in coincidence, thereby differentiating between all breakup channels; $\text{H}^+ + \text{D}$, $\text{H} + \text{D}^+$, or $\text{H}^+ + \text{D}^+$. This has the additional advantage of giving a good signal-to-noise ratio since only true events are likely to pass all of the timing and momentum

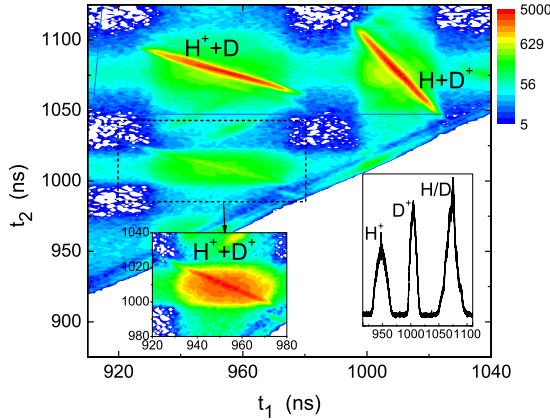


FIG. 2. (Color online) Raw coincidence map of the flight time of the first particle to arrive at the detector (t_1) plotted against the flight time of the second (t_2), showing islands due to the different breakup channels as labeled. Note that the sharp lines are real event pairs that conserve momentum while the surrounding blobs are random coincidences between uncorrelated particles which mostly are eliminated after data processing (see text). The inset on the right shows the 1D time of flight where the H⁺, D⁺, and neutral fragments are all clearly separated.

conservation gates imposed on the raw data when processing and analyzing the data. An example of a coincidence map before data processing, in which each of the channels is distinctly separated, is shown in Fig. 2.

The laser used is a 790 nm (fundamental) Ti:sapphire system utilizing chirped-pulse amplification and a multipass amplifier. This delivers 2 mJ and 35 fs pulses at a 1 kHz repetition rate. To frequency double the pulses a type-I β barium borate (BBO) crystal (250 μ m thickness) is used. This generates 200 μ J and 40 fs second-harmonic (395 nm) pulses that we separate from the fundamental beam using a dichromatic beamsplitter. The polarization direction of the laser is controlled using a half-wave plate positioned prior to the BBO crystal, while the pulse energy is attenuated using neutral density filters, also placed before the BBO crystal. The pulses are focused onto the HD⁺ ion-beam target using a 90° off-axis parabolic mirror, with a focal length $f=203$ mm, mounted to a multidimensional actuator stage. Typical spectra were each recorded for ~ 12 h data-acquisition time, demanding good laser and ion-beam stability.

III. RESULTS AND DISCUSSION

A. Floquet picture

One commonly used approach to gain insight into the dissociation of simple molecules is the Floquet picture. This method describes the nonperturbative interaction of the laser field with the molecule, allowing for the coupling between them. Since a detailed outline of the method may be found elsewhere (e.g., [69,70]), for brevity, we only summarize the main concept here.

When the 395 nm laser interacts with HD⁺, it couples the lowest electronic $1s\sigma$ (ground) and $2p\sigma$ (excited) states. In general, these states are normally considered to be well iso-

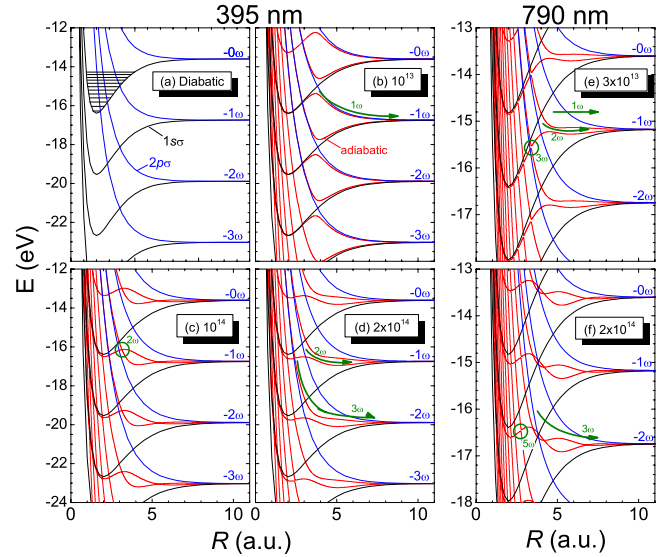


FIG. 3. (Color online) (a) Diabatic Born-Oppenheimer potentials of HD⁺, dressed by net absorbed number of photons, $n\omega$, at 395 nm. The horizontal lines are the calculated unperturbed lowest vibrational levels. [(b)–(d)] Same as (a) with additional curves (thinner red lines) for the adiabatic Floquet potentials at (b) 10^{13} , (c) 10^{14} , and (d) 2×10^{14} W/cm². [(e) and (f)] Same as (b) for 790 nm at (e) 3×10^{13} and (f) 2×10^{14} W/cm². The arrows and labels denote significant pathways of importance for the discussion in the text.

lated from the much higher-lying excited states (~ 10 eV) at intensities below $\sim 5 \times 10^{13}$ W/cm² [30]. Since the electric field of the laser is periodic (determined by the laser carrier frequency), the laser-molecule interaction is modulated with the same periodicity (assuming the laser pulse is long with respect to the laser-cycle period, e.g., 40 fs \gg 1.3 fs for the 395 nm pulses used here.) Thus, the Floquet method transforms the time-dependent Schrödinger equation into an infinite set of time-independent equations using a Fourier series expansion. In this expansion each neighboring Fourier term is coupled.

A consequence of the Floquet approach is the dressed-state picture (e.g., [24]) illustrated in Fig. 3. In Fig. 3(a) the $1s\sigma$ and $2p\sigma$ states are “dressed” in energy by an integer number of photons absorbed or emitted. Thus, the system retains the periodicity of the laser. Where two states cross one another transitions between states are more likely. This is because the two states are spaced by exactly a multiple of the photon energy and are, therefore, resonant. The scenario demonstrated in Fig. 3(a) represents the diabatic limit where the interaction of the laser is weak ($\lesssim 10^{12}$ W/cm²), thus the coupling terms are small. In essence, this diabatic picture is the same as representing the excitation between two states as a vertical transition, resonant with an integer number of photons, in the undressed picture (e.g., [71]). With an increase in intensity, the avoided crossings between states in the dressed-state picture repel one another more strongly, forming an avoided crossing and producing a visible gap as observed in Fig. 3(b) at 10^{13} W/cm². The new curves are the adiabatic curves. A bound molecular wave packet moving on such a potential with sufficient energy to overcome the laser-

induced barrier at the gap between the $|1s\sigma-0\omega\rangle$ and $|2p\sigma-1\omega\rangle$ curves (i.e., the 1ω crossing) will follow the adiabatic pathway and dissociate. This is the process of BS. For HD^+ at 395 nm, the $v=6$ vibrational state is nearest resonance with the 1ω crossing and will dissociate with a KER of ~ 1.75 eV—the difference in energy between the $v=6$ state and the asymptotic one-photon dissociation limit.

When the laser intensity increases to 10^{14} W/cm² [Fig. 3(c)], the 1ω crossing becomes so distorted that it is almost unrecognizable. The progression in intensity to this value from 10^{13} W/cm² reduces the lower potential barrier at the 1ω crossing enabling population of the low vibrational states ($v \approx 1-5$) to escape. The potential above the crossing is also heightened allowing population in states above the crossing to also dissociate. Hence, these changes are accompanied by a spread in the kinetic energy released. At 10^{14} W/cm² the next higher photon ($n\omega$) crossing, i.e., the 2ω crossing between the $|1s\sigma-0\omega\rangle$ and $|2p\sigma-2\omega\rangle$ curves, is still visibly closed. It is not until $\sim 2 \times 10^{14}$ W/cm² [Fig. 3(d)] that the strong repulsion at the net 1ω crossings, $|1s\sigma-0\omega\rangle-|2p\sigma-1\omega\rangle$ and $|1s\sigma-1\omega\rangle-|2p\sigma-2\omega\rangle$, forces the 2ω crossing to open. However, rather than leading to the direct two-photon dissociation limit, the adiabatic path is to the one-photon limit through stimulated emission of a photon. Hence, under normal circumstances [72], one cannot expect to observe direct two-photon dissociation of HD^+ at 395 nm. We also begin to see signs of opening of the 3ω crossing at 2×10^{14} W/cm². The adiabatic pathway proceeding from this crossing is steep and leads to the two-photon dissociation limit. The expected KER will be on the order of 4–6 eV dependent on the dissociating vibrational state. To observe opening of higher $n\omega$ crossings, one needs to go to much higher intensities ($>10^{15}$ W/cm²). However, at such intensities excitation to higher-lying electronic states and ionization will play a bigger role in the dynamics. To avoid this we limit our study to $\leq 2 \times 10^{14}$ W/cm².

B. 395 nm dissociation spectra

The experimental results for the dissociation of HD^+ at a selection of intensities are shown in Fig. 4. Here we display dissociation to the H^++D channel, but note that the dissociation spectra for the corresponding channel, $\text{H}+\text{D}^+$, are the same within experimental uncertainty. The plots in Figs. 4(a)–4(d) are KER- $\cos\theta$ distributions, displaying both the angular and kinetic-energy release information. The angle θ is the angle between the molecular fragmentation axis and the laser polarization and is binned in $\cos\theta$ since an isotropic spherical distribution will be uniform in that representation. Although Figs. 4(a)–4(c) only cover a small range of intensities from 10^{14} – 2×10^{14} W/cm², significant differences in the spectra are observed.

At 10^{14} W/cm² [Fig. 4(c)], the KER- $\cos\theta$ distribution is peaked at 1.70 eV, evident also from the one-dimensional (1D) KER projection in Fig. 5, integrated for all angles. This value is in good agreement with the expected KER from dissociation of the $v=6$ state (1.75 eV) that is near resonant with the 1ω crossing on the diabatic Floquet picture. For dissociation with this KER value (integrated between 1.7 and

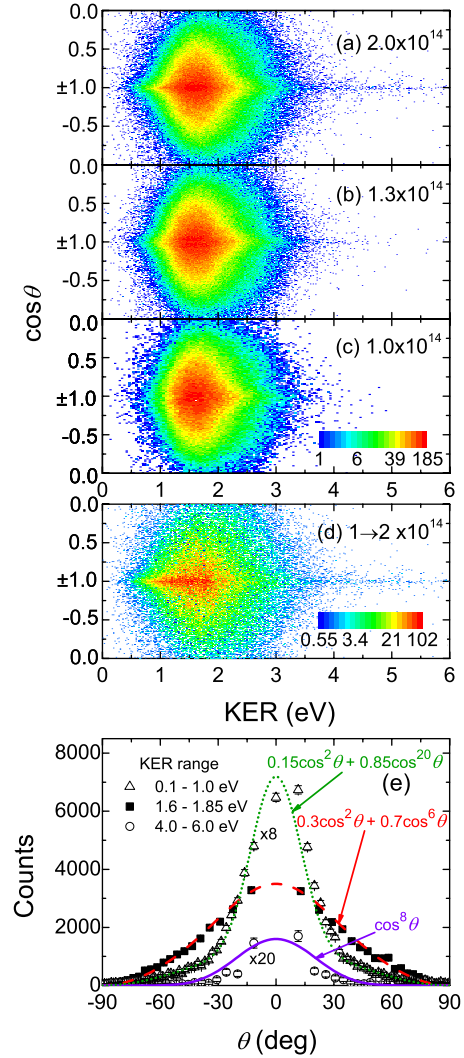


FIG. 4. (Color online) Plots (a–c): Measured KER- $\cos\theta$ distributions for the dissociation of HD^+ to H^++D using 395 nm, 40 fs pulses at intensities (a) 2×10^{14} , (b) 1.3×10^{14} , and (c) 10^{14} W/cm². Plot (d): IDS for the intensity range 10^{14} – 2×10^{14} W/cm², i.e., plot (c) subtracted from plot (a). Plot (e): angular distribution corresponding to the IDS spectra in (d) for KER ranges indicated. The curves are fits to the data. Error bars in (e) are the statistical error of the data.

1.8 eV), the angular distribution of the fragments is fairly broad giving $\langle \cos^2\theta \rangle = 0.57 \pm 0.01$. It shows that the fragmentation closely follows the $\cos^2\theta$ distribution predicted for a pure one-photon transition, i.e., $\langle \cos^2\theta \rangle = 0.6$. Note that the angular distribution for an n -photon $\sigma \rightarrow \sigma$ transition, i.e., $\Delta\Lambda = 0$, is approximately given by $\cos^{2n}\theta$ [66,73].

The angular trend on either side of the KER peak can also be explained within the Floquet picture by BS. Figure 3 shows that with increasing intensity the 1ω crossing gap widens. This releases vibrational states above and below the crossing leading to dissociation with KER greater than and less than the KER associated with the crossing (1.75 eV). For molecules to experience the high intensities required to widen the 1ω crossing they need to be closely aligned to the laser field, i.e., for parallel transitions, the effective intensity is given by $I_{\text{eff}} = I \cos^2\theta$, where I is the laser intensity.

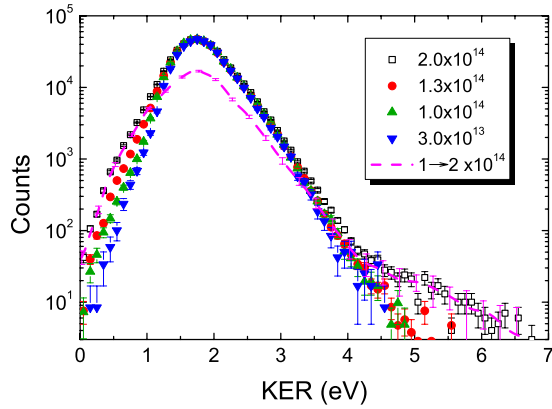


FIG. 5. (Color online) KER distributions, integrated for all angles, for the dissociation of HD⁺ to H+D⁺ at intensities indicated in units of W/cm², normalized to their peak counts. The dashed curve is the intensity-difference spectrum for the intensity range 10^{14} – 2×10^{14} W/cm². Error bars are the statistical error of the data.

Therefore, through this geometric-alignment effect [74,75] the angular distribution for dissociation becomes narrower along the laser polarization for KER on either side of the crossing value. This is observed in Fig. 4(c) in the form of a diamondlike shape in the KER- $\cos \theta$ plot centered about 1.7 eV.

The high KER cutoff in Fig. 4(c) extends just above 3 eV. This is close to the maximum value permitted for one-photon dissociation, which results from dissociation of high vibrational states near the continuum with KER equal to the photon energy (3.1 eV).

Comparing the spectra at 1.3×10^{14} [Fig. 4(b)] and 2.0×10^{14} W/cm² [Fig. 4(a)] with the spectra at 10^{14} W/cm², the KER- $\cos \theta$ distribution clearly develops a more sharply aligned feature extending to high KER (up to ~ 6 eV) in addition to the broader low-KER feature present at low intensity. The continued presence of the broad low-KER feature at 2×10^{14} W/cm² is due to volume-averaging effects within the laser focus. That is, the highest intensity is only experienced by molecules contained within a small volume at the very center of the laser focus. Lower intensity focal shells surrounding this region (with larger volume) will contribute to low intensity dissociation of HD⁺. To circumvent this effect, we have previously developed an IDS technique [65,76] that effectively subtracts the low intensity contributions from a higher intensity measurement by taking the difference between the spectra from the low and high intensity measurements. We have applied this technique here to observe the changes from 10^{14} to 2.0×10^{14} W/cm² as demonstrated in Fig. 4(d). Largely the broad low-KER feature is suppressed revealing an underlying more sharply aligned ridge.

There are two interesting aspects to this sharply aligned feature. First, it extends in KER to nearly 6 eV. Such an energy release can only come from above-threshold dissociation channels. Referring to Fig. 3, for net three-photon ATD one would expect a minimum KER of ~ 7 eV which is too large to explain the observed value. Rather, the net two-photon pathway marked in Fig. 3(e) that follows the adia-

batic route from the 3ω crossing is consistent with a KER value of ~ 3.7 eV for dissociation of $v=0$, with higher KER gained from dissociation of higher- v states. Measuring the angular distribution of the fragments in the KER range 4.0–6.0 eV, one obtains $\langle \cos^2 \theta \rangle = 0.80 \pm 0.05$. This value fits well with a $\cos^8 \theta$ distribution, which gives $\langle \cos^2 \theta \rangle = 0.82$, expected for the $|1s\sigma-0\omega\rangle \rightarrow |2p\sigma-3\omega\rangle \rightarrow |1s\sigma-2\omega\rangle$ pathway, i.e., $\cos^6 \theta \cos^2 \theta$. A plot of the angular distribution for the high KER slice shown in Fig. 4(e) confirms this assignment where a $\cos^8 \theta$ fit shows fair agreement. By careful inspection of the Floquet diagram in Fig. 3(d) it is evident that the 3ω crossing is open at 2×10^{14} W/cm². There is a small but distinct gap at this crossing. The fact that the fragmentation is highly aligned to the laser field is again caused by the need for high effective field strength along the molecular axis, i.e., geometric alignment, to open the gap leading to this pathway.

The second aspect of the sharply aligned feature is that it also extends to low KER, below 0.5 eV, which cannot arise from the aforementioned pathway through the 3ω crossing. It would seem that dissociation instead could come from either BS of the direct one-photon pathway, $|1s\sigma-0\omega\rangle \rightarrow |2p\sigma-1\omega\rangle$, or through the net one-photon pathway via the 2ω crossing, $|1s\sigma-0\omega\rangle \rightarrow |2p\sigma-2\omega\rangle \rightarrow |1s\sigma-1\omega\rangle$, although we suspect this latter pathway will be weak at 395 nm wavelength. We also note that this latter pathway is only present for HD⁺ and is absent for H₂⁺ and D₂⁺ as the symmetry of the homonuclear molecules forbids the direct absorption of two photons, i.e., this pathway involves a permanent dipole transition. While the Floquet potentials in Fig. 3(d) indicate that the $|1s\sigma-0\omega\rangle \rightarrow |2p\sigma-2\omega\rangle \rightarrow |1s\sigma-1\omega\rangle$ pathway is open at 2×10^{14} W/cm², the expected KER would be ~ 0.9 eV from the position of the diabatic crossing. This only roughly agrees with the observed KER, which is mainly between 1.0–2.0 eV with a weaker component extending to below 0.5 eV.

To further investigate the origin of this highly aligned feature, we plot in Fig. 4(e) the 1D angular distribution integrated for three KER ranges, 1.6–1.85 eV and 0.1–1.0 eV, in addition to the range 4.0–6.0 eV already discussed. In the KER range 1.6–1.85 eV we expect only direct 1ω dissociation of states near $v=6$, with no contribution from the 2ω crossing. Good agreement with the data in this KER range is achieved with a combination of a $\cos^2 \theta$ and a $\cos^6 \theta$ fit. As discussed, $\cos^2 \theta$ normally denotes a direct one-photon transition and may come from molecules dissociating on the low intensity leading edge of the laser pulse. The additional $\cos^6 \theta$ component seems to indicate some dynamic alignment of molecules that survive to the later high-intensity part of the laser pulse. Dynamic alignment in the strong laser field torques the molecules, pulling them into alignment with the polarization, and is more effective at higher intensities.

Below 1.0 eV, the degree of alignment is much higher with a strong $\sim \cos^{20} \theta$ component observed. For the pathway $|1s\sigma-0\omega\rangle \rightarrow |2p\sigma-2\omega\rangle \rightarrow |1s\sigma-1\omega\rangle$ we expect $\cos^6 \theta$ (i.e., $\cos^4 \theta \cos^2 \theta$). However, this will be masked by the competing processes of geometric alignment from one-photon BS of low v states and dynamic alignment as just discussed that can both lead to the high degree of observed alignment. Hence, it is difficult to find a clear signature for

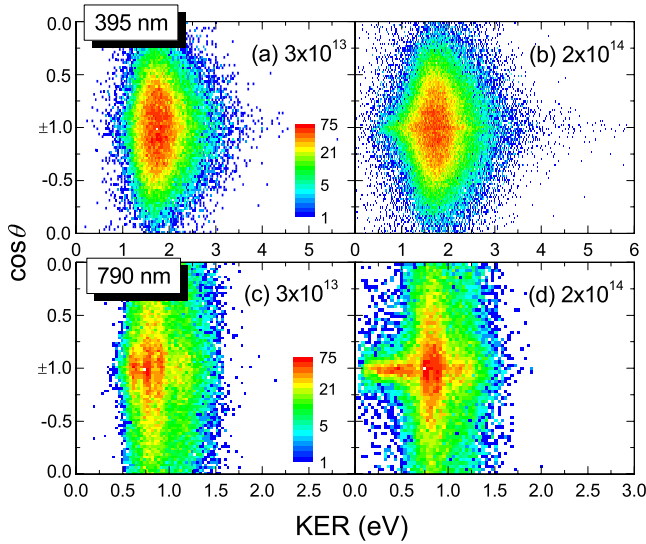


FIG. 6. (Color online) [(a) and (b)] KER- $\cos \theta$ plots for 395 nm at intensities 3×10^{13} and 2×10^{14} W/cm², respectively. [(c) and (d)] Same as (a) and (b), respectively, for 790 nm.

dissociation through the 2ω crossing as it is not well separated energetically from other processes.

To explicitly observe the changes in the spectra with intensity, we overlay the KER distributions for the H + D⁺ channel for each intensity, plus an additional measurement at 3×10^{13} W/cm², as shown in Fig. 5. Figure 5 clearly highlights the high KER (>4 eV) shoulder observed at 2×10^{14} W/cm² and the broadening of the distribution to low KER (<1 eV) with increasing intensity. Overall, we can conclude that, below 10^{14} W/cm², BS of states near $v=6$ dominates dissociation. Above 10^{14} W/cm², BS allows lower v states to dissociate while some dynamic alignment occurs. Above-threshold dissociation from the 3ω crossing with the ground state also begins to contribute to the dissociation although it is difficult to say whether there is any dissociation from the 2ω crossing as it overlaps in KER with BS.

C. Comparison of 395 and 790 nm dissociation

In Fig. 6 we compare data for dissociation using the fundamental (790 nm) and second-harmonic (395 nm) wavelengths at similar pulse duration (35 fs for 790 nm; 40 fs for 395 nm). The spectra shown in Fig. 6 are for the H+D⁺ channel at 3×10^{13} and 2×10^{14} W/cm², while the H⁺+D channel is similar. At 790 nm, structure in the KER- $\cos \theta$ plots is observed from dissociation of different vibrational states. This structure might also be present at 395 nm but the energy resolution of that experiment was poorer. Aside from the vibrational structure, the 790 and 395 nm distributions at 3×10^{13} W/cm² share some similar features. For example, the largest peak at 790 nm appears at KER=0.77 eV as expected for one-photon dissociation of $v=10$ (the v state nearest the 1ω crossing). Similarly the 395 nm distribution is peaked at KER=1.7 eV due to near resonance one-photon dissociation of $v=6$. At these energies, both distributions fit a $\cos^2 \theta$, and become narrower in angle on either side due to

the geometrical alignment of BS (see discussion in previous section).

Inspection of the Floquet potentials for 790 nm, 3×10^{13} W/cm² in Fig. 3(e) confirms that the 1ω crossing is wide open from BS. The Floquet picture also reveals that already at 3×10^{13} W/cm² the 2ω crossing is significantly open with the adiabatic pathway $|1s\sigma-0\omega\rangle \rightarrow |2p\sigma-2\omega\rangle \rightarrow |1s\sigma-1\omega\rangle$ leading to net one-photon dissociation. The equivalent pathway does not open until almost 2×10^{14} W/cm² in the Floquet diagram at 395 nm [Fig. 3(d)]. Despite being open at 790 nm, we do not observe any dissociation through the 2ω crossing as it would result in very low KER (below 0.5 eV), which is absent in Fig. 6(c). This absence perhaps confirms our suspicion that at 395 nm we also do not see a clear signature of this channel. Theoretical investigation is required to help determine why.

At 2×10^{14} W/cm², the 790 nm distribution develops a low KER nose similar to 395 nm data. At 395 nm we assigned this nose predominantly to one-photon dissociation from the 1ω crossing, although we could not distinguish if there were also contributions from the 2ω crossing. For 790 nm we can expect similar contributions. In addition, though, the Floquet potentials for 790 nm [Fig. 3(f)] show that the 3ω crossing is open and leads to net two-photon dissociation. The KER from these pathways will also be low and overlap with the low KER from one-photon dissociation.

Unlike 395 nm, the formation of the high KER tail is absent for 790 nm. In the case of 395 nm, this tail resulted from net two-photon dissociation via $|1s\sigma-0\omega\rangle \rightarrow |2p\sigma-3\omega\rangle \rightarrow |1s\sigma-2\omega\rangle$. To observe a similar feature for 790 nm would require net three-photon dissociation, as both net one- and net two-photon dissociation lead to low KER (≤ 1.6 eV). Since the adiabatic pathway from the 4ω crossing also leads to net two-photon dissociation, to observe net three-photon dissociation requires opening of the 5ω crossing, i.e., $|1s\sigma-0\omega\rangle \rightarrow |2p\sigma-5\omega\rangle \rightarrow |1s\sigma-3\omega\rangle$. This does not occur until $\sim 3 \times 10^{14}$ W/cm², therefore, it is not surprising that the high KER tail is missing at 790 nm.

The main conclusion that we can draw from the 395 and 790 nm comparison is that for the same given intensity the gaps at the avoided crossings of the adiabatic Floquet potentials are wider open at the longer wavelength, as shown in Fig. 3. This is because below 10 a.u. the transition dipole moment of HD⁺ decreases for smaller internuclear distances, R , and at 395 nm the dressed-state curve crossings of $1s\sigma$ and $2p\sigma$ occur at smaller R than at 790 nm. Thus, as is supported by the data presented here, for a given intensity it is more difficult for HD⁺ to dissociate along a certain pathway at 395 nm than at 790 nm.

This conclusion is rather fascinating as it is in direct contradiction to that seen in ionization. The appearance intensity for HD⁺ ionization is lower for 395 nm than for 790 nm due to the need to absorb fewer photons, i.e., half as many, to reach the same position on the ionization, $1/R$, potential energy curve at 395 nm. For example, in our measurements the onset of ionization of HD⁺ occurs at $\sim 1.3 \times 10^{14}$ W/cm² for 395 nm, compared with $\sim 2.5 \times 10^{14}$ W/cm² for 790 nm (in agreement with H₂⁺ [53]).

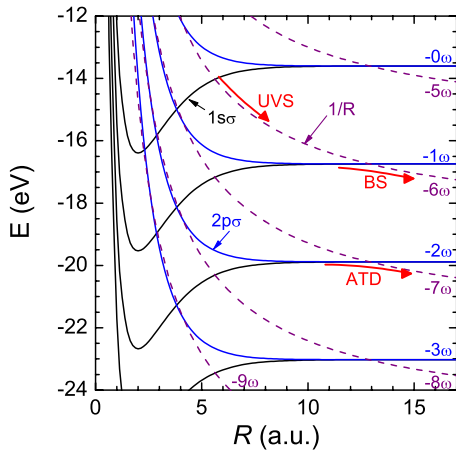


FIG. 7. (Color online) Dressed-states diagram of HD⁺ at 395 nm wavelength including both the dissociation (solid) and ionization (dashed) curves. UVS, BS, and ATD indicate ionization pathways that are initiated by dissociation of the UVSs and the processes of BS and ATD (see text).

D. Above-threshold Coulomb explosion

In previous work on an H₂⁺ ion beam, our group observed structure in the KER spectra for ionization, both for 395 and 790 nm wavelengths [56]. It was found that this structure was most prominent near the appearance intensity for multiphoton ionization. The structure was attributed to above-threshold Coulomb explosion [56]—ionization via above-threshold pathways, much like those for ATD. Shortly after this discovery, an alternative explanation based on interference effects from two dissociation paths was used to explain apparently similar structure when starting from an H₂ target [40,77]. If the origin of these structures is the same, the question of which model is more appropriate has yet to be resolved.

Since the two-pathway interference explanation involves two coherent wave packets, it would seem less applicable in the present ion-beam study where the HD⁺ molecules are initially vibrationally incoherent. Therefore, we will focus here only on the ATCE model. Perhaps the most powerful feature of this model is its simplicity and ability to predict *a priori* the position and trend in widths of KER peaks.

To begin, we revisit the diabatic Floquet picture used in Fig. 3(a). Up to now we have only discussed this picture in the context of dissociation. However, in principle, we can also incorporate the laser-dressed ionization potentials ($1/R$) as outlined in Ref. [56]. This combined Floquet picture including dissociation and ionization together will only work well near the threshold for ionization, i.e., when channels first begin to open. In Fig. 7 we illustrate this unified Floquet diagram. The $1/R$ repulsive potential of the transient HD²⁺ has been dressed by the necessary number of photons to achieve ionization (~ 5 – 8 photons). As before, where the different curves cross one another, transitions between states are possible. Due to the complex network of crossings in this picture, there are a number of different ionization pathways. To simplify, we categorize these into three forms—ionization that occurs from (i) the upper vibrational states (UVSs)

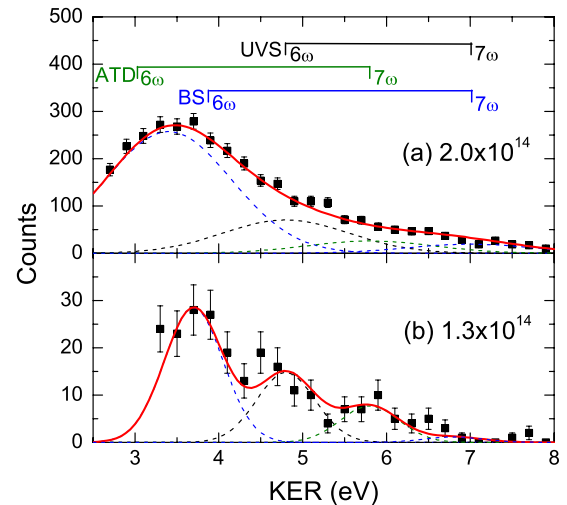


FIG. 8. (Color online) KER distributions for ionization of HD⁺ to H⁺+D⁺ at (a) 2.0×10^{14} and (b) 1.3×10^{14} W/cm². The tick marks with labels indicate expected positions of peaks due to different ionization pathways, see text. The data (solid points) have been fitted with Gaussian peaks (dashed curves) as discussed in the text. The solid curves are the sum of these fits. The error bars are the statistical error of the data.

above the 1ω crossing, (ii) bond softening (BS) or (iii) above-threshold dissociation (ATD). That is, UVS simply refers to ionization resulting from direct crossings of the $1/R$ curve with high- ν states above the 1ω crossing, and BS and ATD refer to dissociation from crossings of the $1/R$ curve with BS- and ATD-instigated dissociation pathways. To find the expected KER from these pathways we simply take the energy difference between where the start of the pathway crosses the $|1s\sigma-0\omega\rangle$ ground state, and where the pathway ends at the ionization limit $R=\infty$ on the $|1/R-n\omega\rangle$ state. For example, consider ionization along the ATCE pathway denoted BS in Fig. 7, i.e., $|1s\sigma-0\omega\rangle \rightarrow |2p\sigma-1\omega\rangle \rightarrow |1/R-6\omega\rangle$. For the initial dissociation step along $2p\sigma$ between $R=3.8$ and 13.0 a.u., the energy release is 1.75 eV. In the second step involving ionization at $R=13.0$ a.u. an additional 2.10 eV is released. Therefore, we expect to observe a KER peak centered at 3.85 eV. Following this simple logic one can predict the approximate energies of all the KER peaks.

We now test these predictions experimentally. In Fig. 8 we plot experimental data for the ionization of HD⁺ into H⁺+D⁺ at (a) 2.0×10^{14} and (b) 1.3×10^{14} W/cm². The data are only plotted for a small cone of angles ($|\cos \theta| > 0.95$) along the laser polarization to limit the effects of intensity averaging (unaligned molecules experience lower effective intensity). However, we note that the majority of fragments are emitted within this cone due to the highly aligned nature of ionization. Events below ~ 3 eV are not shown in the figure as below this KER there is a sizable probability of false coincidences between H⁺ and D⁺ ions coming from the much more dominant dissociation channel, therefore leaving some uncertainty in the data.

At 1.3×10^{14} W/cm² [Fig. 8(b)], near the appearance intensity for ionization, there are signatures of peaks in the KER distribution. The positions of these peaks are in reason-

able agreement with the energies predicted using the ATCE model—see labeled tick marks on the upper panel of the figure. Each peak is fitted with a Gaussian distribution whose centroid corresponds to the predicted value, with one exception. For the BS peak we obtain a better fit to the data by allowing a small downward shift in its centroid of <0.2 eV in conjunction with a lowering of the BS dissociation barrier at the 1ω crossing. The width of each Gaussian peak was kept the same to limit the number of free parameters. One observes that the dominant peak, centered at 3.7 eV, originates from BS followed by a crossing with the $|1/R-6\omega\rangle$ curve, i.e., 1-photon+5-photon ionization. As BS is the dominant dissociation mechanism, its important role in ionization is to be expected. On the other hand, the peak at 4.8 eV originates from a direct crossing of the $|1/R-6\omega\rangle$ curve with the ground state above the 1ω crossing, i.e., UVS population (see Fig. 7). Given that the Franck-Condon population residing in the high- v states near this crossing is relatively small (only a few percent) [67,68], it is surprising to find such a large contribution from this pathway. The third main contribution observed, centered at 5.8 eV, originates from net two-photon ATD ($|1s\sigma-0\omega\rangle \rightarrow |2p\sigma-3\omega\rangle \rightarrow |1s\sigma-2\omega\rangle$) that then forms a crossing with the $|1/R-7\omega\rangle$ state. Our results from dissociation (Sec. III B) indicate that this ATD channel begins to open around this intensity which can explain its appearance in the ionization channel.

At slightly higher intensity, 2.0×10^{14} W/cm² [Fig. 8(a)], the distinct peaks in the KER are seen to broaden and effectively wash out. This agrees with a further prediction of the ATCE model: structure will be most prominent near the appearance intensity for ionization. The reason for this is that the curve crossings in Fig. 7 widen with increasing intensity allowing ionization to occur over a larger range of R , adding to the broadening of the KER peaks and eventually washing them out. We note also a small shift (~ 0.3 eV) of the BS peak to even lower KER as the BS dissociation barrier is lowered further at higher intensity. Overall, the broad structure seen in Fig. 8(a) looks remarkably similar to that observed previously for H₂⁺ under similar conditions [56], reaffirming the presence of ATCE peaks for 395 nm wavelength.

One further point of interest is that for the dominant ATCE pathways, the last step, involving resonant ionization to the $1/R$ curve, occurs at large R (>5 a.u.) as this requires the absorption of fewer photons. This is the reason for the moderate KER (<7 eV) observed for ionization compared

with that expected (~ 14 eV) should ionization occur at small $R=2$ a.u.. In the past when relatively low KER of this nature has been observed it has typically been assigned to charge-resonance enhanced ionization (CREI) for stretched molecules at some critical internuclear distance(s) R_c larger than the molecule's equilibrium distance (for H₂⁺, $R_c \sim 6-10$ a.u. [34,43,78]). Our results show that the low KER may alternatively be explained using the ATCE model.

IV. SUMMARY

In summary, the fairly recent introduction of hydrogen molecular-ion beam studies to intense laser fields has helped to fill a void in knowledge of how small molecules couple with the laser field. So far these studies have been concentrated near 800 nm. In the absence of an earlier detailed investigation, we have explored the dissociation and ionization of a HD⁺ beam using intense 395 nm, 40 fs laser pulses as a function of laser intensity in the interval $3 \times 10^{13} - 2 \times 10^{14}$ W/cm². Different fragmentation channels were separated using coincidence 3D momentum imaging providing kinetic-energy release and angular distributions. The results show the onset of above-threshold dissociation above $\sim 10^{14}$ W/cm², with the fragments emitted strongly along the laser polarization. The ATD comes from the $|1s\sigma-0\omega\rangle \rightarrow |2p\sigma-3\omega\rangle \rightarrow |1s\sigma-2\omega\rangle$ pathway. We do not observe a clear signature for dissociation due to the 2ω crossing in HD⁺ from permanent dipole transitions, neither at 395 nm nor 790 nm. In general, the behavior at 790 and 395 nm is qualitatively similar although interestingly it is found that dissociation processes appear at lower intensities for 790 nm despite having a higher ionization threshold. In the ionization spectra at 395 nm there is evidence of structure, consistent with our earlier proposed above-threshold Coulomb explosion interpretation.

ACKNOWLEDGMENTS

The authors wish to thank Professor Z. Chang and his group members for providing the laser beam and Dr. C. W. Fehrenbach for assistance with the ion beam. This work was supported by the Chemical Sciences, Geosciences, and Biosciences Division, Office of Basic Energy Sciences, Office of Science, U.S. Department of Energy.

-
- [1] J. H. Posthumus, Rep. Prog. Phys. **67**, 623 (2004).
 [2] A. McPherson, G. Gibson, H. Jara, U. Johann, T. S. Luk, I. A. McIntyre, K. Boyer, and C. K. Rhodes, J. Opt. Soc. Am. B **4**, 595 (1987).
 [3] H. Stapelfeldt and T. Seideman, Rev. Mod. Phys. **75**, 543 (2003).
 [4] M. F. Kling, C. Siedschlag, A. J. Verhoef, J. I. Khan, M. Schultze, Th. Uphues, Y. Ni, M. Uiberacker, M. Drescher, F. Krausz *et al.*, Science **312**, 246 (2006).
 [5] J. Itatani, J. Levesque, D. Zeidler, H. Niikura, H. Pépin, J. C. Kieffer, P. B. Corkum, and D. M. Villeneuve, Nature (London) **432**, 867 (2004).
 [6] M. Meckel, D. Comtois, D. Zeidler, A. Staudte, D. Pavičić, H. C. Bandulet, H. Pépin, J. C. Kieffer, R. Dörner, D. M. Villeneuve *et al.*, Science **320**, 1478 (2008).
 [7] P. H. Bucksbaum, A. Zavriyev, H. G. Muller, and D. W. Schumacher, Phys. Rev. Lett. **64**, 1883 (1990).
 [8] F. Légaré, I. V. Litvinyuk, P. W. Dooley, F. Quéré, A. D. Bandrauk, D. M. Villeneuve, and P. B. Corkum, Phys. Rev. Lett. **91**, 093002 (2003).
 [9] A. Rudenko, B. Feuerstein, K. Zrost, V. L. B. de Jesus, Th. Ergler, C. Dimopoulou, C. D. Schröter, R. Moshhammer, and J.

- Ullrich, J. Phys. B **38**, 487 (2005).
- [10] C. Trump, H. Rottke, and W. Sandner, Phys. Rev. A **59**, 2858 (1999).
- [11] J. H. Posthumus, J. Plumridge, P. F. Taday, J. H. Sanderson, A. J. Langley, K. Codling, and W. A. Bryan, J. Phys. B **32**, L93 (1999).
- [12] H. Rehbein, J. Harms, R. Schnabel, and K. Danzmann, Phys. Rev. Lett. **95**, 193001 (2005).
- [13] A. S. Alnaser, B. Ulrich, X. M. Tong, I. V. Litvinyuk, C. M. Maharjan, P. Ranitovic, T. Osipov, R. Ali, S. Ghimire, Z. Chang *et al.*, Phys. Rev. A **72**, 030702(R) (2005).
- [14] Th. Ergler, A. Rudenko, B. Feuerstein, K. Zrost, C. D. Schröter, R. Moshhammer, and J. Ullrich, Phys. Rev. Lett. **97**, 193001 (2006).
- [15] H. Niikura, D. M. Villeneuve, and P. B. Corkum, Phys. Rev. A **73**, 021402(R) (2006).
- [16] K. F. Lee, F. Légaré, D. M. Villeneuve, and P. B. Corkum, J. Phys. B **39**, 4081 (2006).
- [17] W. A. Bryan, J. McKenna, E. M. L. English, J. Wood, C. R. Calvert, R. Torres, D. S. Murphy, I. C. E. Turcu, J. L. Collier, J. F. McCann *et al.*, Phys. Rev. A **76**, 053402 (2007).
- [18] B. Feuerstein, Th. Ergler, A. Rudenko, K. Zrost, C. D. Schröter, R. Moshhammer, J. Ullrich, T. Niederhausen, and U. Thumm, Phys. Rev. Lett. **99**, 153002 (2007).
- [19] W. A. Bryan, E. M. L. English, J. McKenna, J. Wood, C. R. Calvert, I. C. E. Turcu, R. Torres, J. L. Collier, I. D. Williams, and W. R. Newell, Phys. Rev. A **76**, 023414 (2007).
- [20] A. Giusti-Suzor, X. He, O. Atabek, and F. H. Mies, Phys. Rev. Lett. **64**, 515 (1990).
- [21] G. Jolicard and O. Atabek, Phys. Rev. A **46**, 5845 (1992).
- [22] E. E. Aubanel, J.-M. Gauthier, and A. D. Bandrauk, Phys. Rev. A **48**, 2145 (1993).
- [23] E. E. Aubanel, A. Conjusteau, and A. D. Bandrauk, Phys. Rev. A **48**, R4011 (1993).
- [24] A. Giusti-Suzor, F. H. Mies, L. F. DiMauro, E. Charron, and B. Yang, J. Phys. B **28**, 309 (1995).
- [25] A. Zavriyev, P. H. Bucksbaum, J. Squier, and F. Saline, Phys. Rev. Lett. **70**, 1077 (1993).
- [26] L. J. Frasinski, J. H. Posthumus, J. Plumridge, K. Codling, P. F. Taday, and A. J. Langley, Phys. Rev. Lett. **83**, 3625 (1999).
- [27] F. Anis and B. D. Esry, Phys. Rev. A **77**, 033416 (2008).
- [28] J. H. Posthumus, J. Plumridge, L. J. Frasinski, K. Codling, E. J. Divall, A. J. Langley, and P. F. Taday, J. Phys. B **33**, L563 (2000).
- [29] L. J. Frasinski, J. Plumridge, J. H. Posthumus, K. Codling, P. F. Taday, E. J. Divall, and A. J. Langley, Phys. Rev. Lett. **86**, 2541 (2001).
- [30] J. McKenna, A. M. Sayler, F. Anis, B. Gaire, N. G. Johnson, E. Parke, J. J. Hua, H. Mashiko, C. M. Nakamura, E. Moon *et al.*, Phys. Rev. Lett. **100**, 133001 (2008).
- [31] P. Agostini, F. Fabre, G. Mainfray, G. Petite, and N. K. Rahman, Phys. Rev. Lett. **42**, 1127 (1979).
- [32] J. Posthumus, L. Frasinski, A. Giles, and K. Codling, J. Phys. B **28**, L349 (1995).
- [33] K. Codling and L. Frasinski, J. Phys. B **26**, 783 (1993).
- [34] T. Zuo and A. D. Bandrauk, Phys. Rev. A **52**, R2511 (1995).
- [35] T. Seideman, M. Y. Ivanov, and P. B. Corkum, Phys. Rev. Lett. **75**, 2819 (1995).
- [36] S. Chelkowski and A. D. Bandrauk, J. Phys. B **28**, L723 (1995).
- [37] A. D. Bandrauk, *Molecules in Intense Laser Fields* (Marcel Dekker, New York, 1994).
- [38] H. Yu and A. D. Bandrauk, J. Chem. Phys. **102**, 1257 (1995).
- [39] P. Dietrich, M. Y. Ivanov, F. A. Ilkov, and P. B. Corkum, Phys. Rev. Lett. **77**, 4150 (1996).
- [40] S. Chelkowski, A. Conjusteau, T. Zuo, and A. D. Bandrauk, Phys. Rev. A **54**, 3235 (1996).
- [41] A. Conjusteau, A. D. Bandrauk, and P. B. Corkum, J. Chem. Phys. **106**, 9095 (1997).
- [42] F. Châteauneuf, T.-T. Nguyen-Dang, N. Ouellet, and O. Atabek, J. Chem. Phys. **108**, 3974 (1998).
- [43] L. Y. Peng, D. Dundas, J. F. McCann, K. T. Taylor, and I. D. Williams, J. Phys. B **36**, L295 (2003).
- [44] A. D. Bandrauk, S. Chelkowski, and I. Kawata, Phys. Rev. A **67**, 013407 (2003).
- [45] B. Feuerstein and U. Thumm, Phys. Rev. A **67**, 043405 (2003).
- [46] V. Roudnev, B. D. Esry, and I. Ben-Itzhak, Phys. Rev. Lett. **93**, 163601 (2004).
- [47] L.-Y. Peng, I. D. Williams, and J. F. McCann, J. Phys. B **38**, 1727 (2005).
- [48] J. J. Hua and B. D. Esry, Phys. Rev. A **78**, 055403 (2008).
- [49] K. Sändig, H. Figger, and T. W. Hänsch, Phys. Rev. Lett. **85**, 4876 (2000).
- [50] I. D. Williams, P. McKenna, B. Srigengan, I. M. G. Johnston, W. A. Bryan, J. H. Sanderson, A. El-Zein, T. R. J. Goodworth, W. R. Newell, P. F. Taday *et al.*, J. Phys. B **33**, 2743 (2000).
- [51] D. Pavičić, A. Kiess, T. W. Hänsch, and H. Figger, Phys. Rev. Lett. **94**, 163002 (2005).
- [52] D. Pavičić, T. W. Hänsch, and H. Figger, Phys. Rev. A **72**, 053413 (2005).
- [53] I. Ben-Itzhak, P. Q. Wang, J. F. Xia, A. M. Sayler, M. A. Smith, K. D. Carnes, and B. D. Esry, Phys. Rev. Lett. **95**, 073002 (2005).
- [54] P. Q. Wang, A. M. Sayler, K. D. Carnes, J. F. Xia, M. A. Smith, B. D. Esry, and I. Ben-Itzhak, Phys. Rev. A **74**, 043411 (2006).
- [55] P. Q. Wang, A. M. Sayler, K. D. Carnes, J. F. Xia, M. A. Smith, B. D. Esry, and I. Ben-Itzhak, J. Phys. B **38**, L251 (2005).
- [56] B. D. Esry, A. M. Sayler, P. Q. Wang, K. D. Carnes, and I. Ben-Itzhak, Phys. Rev. Lett. **97**, 013003 (2006).
- [57] J. McKenna, M. Suresh, D. S. Murphy, W. A. Bryan, L.-Y. Peng, S. L. Stebbings, E. M. L. English, J. Wood, B. Srigengan, I. C. E. Turcu *et al.*, J. Phys. B **40**, 2607 (2007).
- [58] P. A. Orr, I. D. Williams, J. B. Greenwood, I. C. E. Turcu, W. A. Bryan, J. Pedregosa-Gutierrez, and C. W. Walter, Phys. Rev. Lett. **98**, 163001 (2007).
- [59] A. Kiess, D. Pavičić, T. W. Hänsch, and H. Figger, Phys. Rev. A **77**, 053401 (2008).
- [60] J. McKenna, A. M. Sayler, B. Gaire, N. G. Johnson, M. Zohrabi, K. D. Carnes, B. D. Esry, and I. Ben-Itzhak, J. Phys. B **42**, 121003 (2009).
- [61] M. R. Thompson, M. K. Thomas, P. F. Taday, J. H. Posthumus, A. J. Langley, L. J. Frasinski, and K. Codling, J. Phys. B **30**, 5755 (1997).
- [62] J. H. Posthumus, B. Fabre, C. Cornaggia, N. de Ruelle, and X. Urbain, Phys. Rev. Lett. **101**, 233004 (2008).
- [63] A. Talebpour, K. Vijayalakshmi, A. D. Bandrauk, T. T. Nguyen-Dang, and S. L. Chin, Phys. Rev. A **62**, 042708 (2000).

- (2000).
- [64] B. Sheehy, B. Walker, and L. F. DiMauro, *Phys. Rev. Lett.* **74**, 4799 (1995).
- [65] P. Q. Wang, A. M. Sayler, K. D. Carnes, B. D. Esry, and I. Ben-Itzhak, *Opt. Lett.* **30**, 664 (2005).
- [66] A. M. Sayler, P. Q. Wang, K. D. Carnes, B. D. Esry, and I. Ben-Itzhak, *Phys. Rev. A* **75**, 063420 (2007).
- [67] Z. Amitay, A. Baer, M. Dahan, J. Levin, Z. Vager, D. Zajfman, L. Knoll, M. Lange, D. Schwalm, R. Wester *et al.*, *Phys. Rev. A* **60**, 3769 (1999).
- [68] F. von Busch and G. H. Dunn, *Phys. Rev. A* **5**, 1726 (1972).
- [69] J. H. Posthumus and J. F. McCann, *Molecules and Clusters in Intense Laser Fields* (Cambridge Press, Cambridge, 2001).
- [70] S. I. Chu and D. Telnov, *Phys. Rep.* **390**, 1 (2004).
- [71] G. N. Gibson, L. Fang, and B. Moser, *Phys. Rev. A* **74**, 041401(R) (2006).
- [72] We have recently shown that for short enough pulses one can reduce the stimulated re-emission process that leads back to lower net photon absorption [30].
- [73] A. Hishikawa, S. Liu, A. Iwasaki, and K. Yamanouchi, *J. Chem. Phys.* **114**, 9856 (2001).
- [74] J. H. Posthumus, J. Plumridge, M. K. Thomas, K. Codling, L. J. Frasinski, A. J. Langley, and P. F. Taday, *J. Phys. B* **31**, L553 (1998).
- [75] F. Rosca-Pruna, E. Springate, H. L. Offerhaus, M. Krishnamurthy, N. Farid, C. Nicole, and M. J. J. Vrakking, *J. Phys. B* **34**, 4919 (2001).
- [76] A. M. Sayler, P. Q. Wang, K. D. Carnes, and I. Ben-Itzhak, *J. Phys. B* **40**, 4367 (2007).
- [77] A. Staudte, D. Pavičić, S. Chelkowski, D. Zeidler, M. Meckel, H. Niikura, M. Schöffler, S. Schössler, B. Ulrich, P. P. Rajeev *et al.*, *Phys. Rev. Lett.* **98**, 073003 (2007).
- [78] M. Plummer and J. F. McCann, *J. Phys. B* **29**, 4625 (1996).